Nano Energy 61 (2019) 119–125

Contents lists available at ScienceDirect

Nano Energy

journal homepage: www.elsevier.com/locate/nanoen

Full paper

In-situ formed Li_2CO_3-free garnet/Li interface by rapid acid treatment for dendrite-free solid-state batteries

Hanyu Huo[a,c,d,1], Yue Chen[a,c,1], Ning Zhao[b], Xiaoting Lin[d], Jing Luo[d], Xiaofei Yang[d], Yulong Liu[d], Xiangxin Guo[b,*], Xueliang Sun[d,**]

[a] State Key Laboratory of High Performance Ceramics and Superfine Microstructure, Shanghai Institute of Ceramics, Chinese Academy of Sciences, Shanghai, 200050, China
[b] College of Physics, Qingdao University, Qingdao, 266071, China
[c] University of Chinese Academy of Sciences, Beijing, 100049, China
[d] Department of Mechanical and Materials Engineering, University of Western Ontario, Ontario N6A 5B9, Canada

ARTICLE INFO

Keywords:
Rapid acid treatment
Garnets
Intrinsic interfaces
Solid-state batteries

ABSTRACT

Garnet-type solid-state electrolytes (SSEs) are very promising due to their high ionic conductivities at room temperature and high stability against Li metal. However, the poor garnet/Li interfacial contact caused by Li_2CO_3 surface contaminant can lead to lithium dendrite growth and the performance decay of solid-state batteries (SSBs), which still hinders their practical application. Herein, a universal and simple method of rapid acid treatment is proposed to perfectly remove the surface Li_2CO_3 and retrieve a lithiophilic SSE surface. The SSE/Li interfacial resistance dramatically decreases from 940 Ω cm^2 to 26 Ω cm^2 at 30 °C. The acid treated garnet-SSE pellets exhibit an interfacial resistance comparable to the pellets with various surface coatings. In addition, the intrinsic garnet/Li interface remains stable during cycling, which enables the Li symmetric cells continuously cycle over 700 h under 0.2 mA cm^{-2} at 30 °C. And the $LiFePO_4$/Li and $LiCoO_2$/Li cells with acid treated garnet-SSE show excellent cycle and rate performances after eliminating the surface contaminant. These results indicate that rapid acid treatment not only guides a new understanding for an intrinsic garnet/Li interface but also is a simple and high-efficiency strategy to well address the interfacial issue for SSBs.

1. Introduction

Li-ion batteries (LIBs) are widely applied in portable electronic devices and automotive vehicles along with the rapid development of technology [1]. However, traditional LIBs based on organic liquid electrolytes cannot meet the needs of high energy density owing to their narrow electrochemical window. In comparison, solid-state batteries (SSBs) using solid-state electrolytes (SSEs) have demonstrated promising compatibility with both high-voltage cathodes and electronegative Li metal anodes, thus enhancing the energy density. In addition, the safety issues related to the flammable liquid electrolytes are well addressed with the replacement of SSEs [2,3].

As a key component in SSBs, typical SSEs have been studied for a long time, including lithium phosphorus oxynitride (LiPON) [4], perovskite-type [5], sodium superionic conductor (NASICON)-type [6,7], sulfide-type [8], and garnet-type materials [9]. Among them, garnet-type $Li_7La_3Zr_2O_{12}$ (LLZO) has attracted extensive attentions due to the chemical and electrochemical stabilities against Li metal and high ionic conductivity reaching 1 mS cm^{-1} at room temperature [10,11]. However, the poor interfacial contact with Li metal can lead to a large interfacial resistance [12–14]. Even worse, lithium dendrite growth can easily occur at the grain boundaries and defect sites of LLZO, causing short circuit of the SSBs [15,16].

The poor interface between LLZO and Li metal is commonly attributed to the lithiophobic nature of LLZO. Various interlayers were reported to effectively transform the LLZO surface from lithiophobic to lithiophilic. The working mechanism of the interlayers can be mainly divided into two categories. One is based on alloy reactions between Li and another metal such as Au, Mg [17–19]. Recently, our group modified the Nb-doped LLZO (LLZNO) surface with a Sn thin film. The interfacial resistance decreased from 758 to 46.6 Ω cm^2 due to the formation of a self-limited Li—Sn alloy layer [20]. The other is based on

* Corresponding author.
** Corresponding author.
E-mail addresses: xxguo@qdu.edu.cn (X. Guo), xsun9@uwo.ca (X. Sun).
[1] The authors contributed equal to this work.

https://doi.org/10.1016/j.nanoen.2019.04.058
Received 2 January 2019; Received in revised form 14 April 2019; Accepted 15 April 2019
Available online 17 April 2019
2211-2855/

conversion reaction, such as ZnO and Al_2O_3 [21,22]. As reported by Hu and his colleagues, the interfacial contact between SSE and Li metal can be significantly improved by introducing an Al_2O_3 buffer layer, and the interface resistance was thus greatly reduced to 1 Ω cm^2 at room temperature. However, growing such nano-scale layers by atom layer deposition (ALD) or magnetic sputtering is somewhat complex and expensive thus hindering their practical applications.

Actually, the poor wettability of Li on LLZO is resulted from a thin Li_2CO_3 layer on the LLZO surface. Cheng et al. and Sakamoto et al. reported that the garnet SSEs can easily react with air (CO_2 and H_2O) to form a thin Li_2CO_3 layer on the surface [23,24]. The contact angle between Li and Li_2CO_3 is 142° according to density functional theory (DFT) simulation, leading to the lithiophobic property of LLZO pellets [25]. In addition, Li_2CO_3 not only has a low Li^+ conductivity of 10^{-7} S cm^{-1} at 25 °C but also will decompose at a low voltage of 3.2 V [26]. The conventional strategies to remove Li_2CO_3 include mechanical polishing and high temperature thermal treatment. However, the mechanical polishing cannot completely remove the Li_2CO_3 and may bring additional contamination. High temperature treatments usually require several hours to rise and drop the temperature, which is time-consuming for practical battery manufacturing. And the risk of Li loss in LLZO at high temperature is another issue that leads to impurity phase and poor Li^+ conductivity [27].

Herein, a novel and simple method of rapid acid treatment is proposed to perfectly remove the Li_2CO_3 layer on the $Li_{6.4}La_3Zr_{1.4}Ta_{0.6}O_{12}$ (LLZTO), thus achieving an intrinsic Li/LLZTO interface (Schematic 1). Dipping the LLZTO pellet into 1 M hydrochloric acid (HCl) solution for 30 s can efficiently remove the surface contamination layer and retrieve the pure garnet LLZTO. The intrinsic LLZTO surface is proved to be lithiophilic. A low interfacial resistance against Li was obtained as 26 Ω cm^2. The favorable interface enabled stable Li plating/stripping for over 700 h under a current density of 0.2 mA cm^{-2} at 30 °C. In contrast, the dendrite growth along the grain boundary is clearly observed in Li symmetric cells with aged LLZTO, leading to the short circuit after only several cycles. Using the acid treated LLZTO SSE, full cells with $LiFePO_4$ or $LiCoO_2$ cathodes also exhibited excellent cycling and rate performances.

2. Experimental section

2.1. The process of rapid acid treatment

Tantalum (Ta)-doped garnet LLZTO powders and dense pellets were prepared by our previous work [28]. The obtained LLZTO garnet electrolytes were aged in the air at room temperature for 1 month. 1 M hydrochloric acid (HCl) was obtained by concentrated HCl (12 M) adding certain water. The aged LLZTO (LLZTO-air) pellets were immersed into the HCl solution for different time (10 s, 30 s, 1min, 5 min and 30 min). After that, the acid treated pellets were rapidly washed by ethanol and died by hair dryer.

2.2. Characterizations of material properties

Crystal structure of LLZTO pellets were examined by X-ray diffraction (XRD, Bruker D2 Phaser), using Cu Kα radiation with 2θ in the range of 10°~80° and a step size of 0.02°. Surface and cross-section morphologies of LLZTO pellets were investigated by scanning electron microscopy (SEM, S3400). Fourier transform infrared (FTIR) spectroscopy was conducted using a Bruker Alpha system with a Diamond attenuated total reflection (ATR) window in the range of 4000 to 400 cm^{-1} at a resolution of 4 cm^{-1}. X-ray photoelectron spectroscopy (XPS, ESCALAB-250) measurements was performed to characterize composition of Li_2CO_3 surface contaminant. Raman spectroscopy was carried out with a WITec Alpha 300 Raman microscope instrument.

2.3. Electrochemical performance test

Ionic conductivities of the LLZTO samples after rapid acid treatment (LLZTO-RAT) were measured by an impedance analyzer (Novocontrol Beta High Performance Impedance Analyzer) with an AC current of 10 mV from 0.1 to 20 M Hz in frequency. Thin gold layers on both surfaces of ceramic pellet were performed by magnetic sputtering as electrodes prior to conductivity test. The LLZTO-RAT pellets were sandwiched between two pieces of Li metal to construct the symmetric cells. The cells were heated at 200 °C for 30 min in Ar-gas glovebox before sealing in Swagelok-type cell mold. A pressure of approximately 10 N cm^{-2} was exerted on the ceramic plates via springs to keep a close contact. Electrochemical impedance spectroscopy (EIS) measurements were performed in the frequency range from 1 MHz to 0.1 Hz with an amplitude of 10 mV by an Autolab instrument. Galvanostatic cycling was conducted using an Arbin battery cycler at different current densities at room temperature. Li/LLZTO-air/Li symmetric cells were also fabricated and cycled under the same procedure as a comparison.

The composite cathode was prepared as follows: firstly, 0.3 M Lithium bis(trifluoromethanesulfonyl)imide (LiTFSI, Sigma-Aldrich) was dissolved in ionic liquid (IL) (PY14TFSI, Sigma-Aldrich) to obtain a homogeneous IL-0.3M solution. Then, The $LiFePO_4$ (LFP) or $LiCoO_2$ (LCO), super P conductive additive (SP), Polyvinylidene Fluoride (PVDF) and IL-0.3M with the weight ratio of LFP (LCO): SP: PVDF: IL-0.3M = 8 : 1: 1 : 6 were ground thoroughly in the mortar. Finally, the toothpaste-like slurry was coated on Al foils to form the composite cathode with the active materials of approximately 2 mg cm^{-2}.

3. Results and discussion

The Ta-doped LLZTO pellet was prepared by hot-pressing sintering

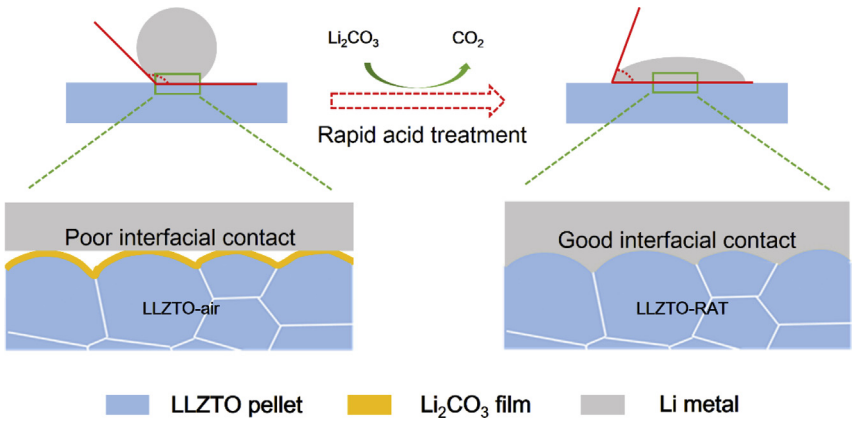

Schematic 1. Schematic illustration of LLZTO/Li interface before and after the rapid acid treatment.

method and exhibited a higher ionic conductivity than pure LLZO [29]. The fabricated LLZTO pellets with a diameter of 12 mm and a thickness of 1 mm were aged in the air for 1 month. This aged LLZTO pellet is abbreviated as LLZTO-air. During this period, the moisture in air can react with LLZTO to form LiOH by Li^+/H^+ ion exchange (equation (1)) [23,25,30].

$$Li_{6.4}La_3Zr_{1.4}Ta_{0.6}O_{12} + x\ H_2O \rightarrow Li_{6.4-x}H_xLa_3\ Zr_{1.4}Ta_{0.6}O_{12} + x\ LiOH \quad (1)$$

And LiOH subsequently reacts with CO_2 to form Li_2CO_3 (equation (2)) on the surface of the LLZTO pellets [31].

$$LiOH + 1/2\ CO_2 \rightarrow 1/2\ Li_2CO_3 + 1/2H_2O \quad (2)$$

According to the transmission electron microscope (TEM) image of LLZTO powder upon the same exposure time in air, the Li_2CO_3 layer on LLZTO-air was estimated to approximately 60-nm thick (Fig. S1). When dipping LLZTO-air into 1 M HCl, bubbles rapidly occurred from the surface of the pellet (Fig. S2) due to release of CO_2 gas (equation (3)).

$$Li_2CO_3 + 2\ HCl \rightarrow 2\ LiCl + CO_2 + H_2O \quad (3)$$

In order to effectively remove Li_2CO_3 to disclose the intrinsic LLZTO surface, different lengths (10 s, 30 s, 1 min, 5 min, 30 min) of acid treatment were investigated. The treated LLZTO-air pellets were referred to as LLZTO-RAT (10 s), LLZTO-RAT (30 s), and LLZTO-RAT (1 min) depending of the treatment time.

X-ray diffraction (XRD) was used to monitor the removal of Li_2CO_3 upon different length of acid treatment. As shown in Fig. 1a, the small Li_2CO_3 peak at approximately 23° gradually disappeared upon acid treatment [32]. After 30 s of acid treatment, the Li_2CO_3 peak was absent, indicating completely removal of Li_2CO_3. No matter with or without acid treatment, all other peaks related to the bulk LLZTO matched well with the standard pattern of cubic-phase LLZO (PDF#45–0109). Further increasing the length of acid treatment to 1, 5 and 30 min, the bulk crystallinity of LLZTO was maintained with no other impurity phases (Fig. S3) [33]. The H^+/Li^+ exchange on the LLZTO surface did not cause a phase change.

Considering that Li has a low X-ray scattering factor, Fourier Transform Infrared Spectoscopy (FT-IR) and Raman spectroscopy were used to identify the Li-containing secondary phases. Fig. 1b compared the FT-IR spectra of LLZTO-air and LLZTO-RATs with different treatment time. V_{as} (C=O) at 1438 and 863 cm^{-1} was consistent with the characteristic peaks of Li_2CO_3 powder. The two obvious peaks on the FT-IR spectrum of LLZTO-air again confirmed the generation of Li_2CO_3 upon exposure to air [34]. As consistent with the XRD results, 30 s of rapid acid treatment had completely removed the Li_2CO_3. The Raman spectra of the untreated and treated LLZTO pellets were shown in Fig. 1c. The peaks at 243, 375, 645, and 728 cm^{-1} were characteristic peaks of the cubic garnet phase, and the first two peaks were related to the Li—O bonding in the garnet structure. All samples exhibited the characteristic peaks of the cubic garnet, indicating no phase change of cubic garnet after acid treatment. Intense peaks at 158 and 1090 cm^{-1} corresponding to the vibration of CO_3^{2-} were observed in LLZTO-air. After acid treatment of 10 s, the intensity of peaks related to Li_2CO_3 decreased due to the partial removal of Li_2CO_3 on the surface of LLZTO-RAT (10 s). Acid treatment for 30 s was enough to clean the Li_2CO_3. In addition, Raman mappings for 900 spots in a 30 × 30 μm^2 area were conducted on the four samples (Fig. 1d). The color indicated the intensity integral calculated from the typical signal of CO_3^{2-} at 1090 cm^{-1}. The LLZTO-air showed strong Raman signals of CO_3^{2-} with uneven distribution, while the Li_2CO_3 cleaning effect of rapid aid treatment was consistent with the XRD and FT-IR results (Figs. 1d and S4).

X-ray photoelectron spectroscopy (XPS) analysis was conducted before and after rapid acid treatment. As shown in Fig. 1e, the two

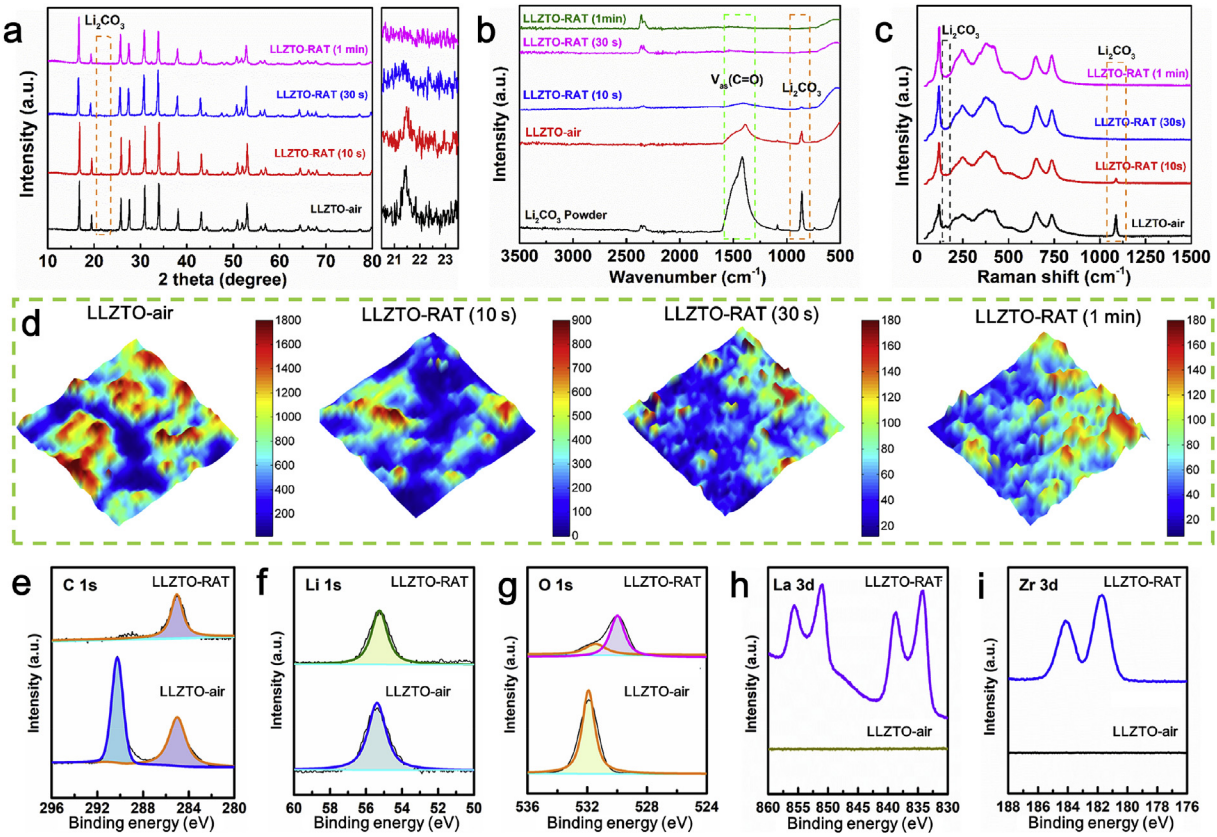

Fig. 1. a) XRD patterns, b) FT-IR spectra, c) Raman spectra, and d) Raman mappings of the aged LLZTO pellet and LLZTO with different acid treated time. e-i) XPS results of LLZT-air and LLZT-RAT (30 s).

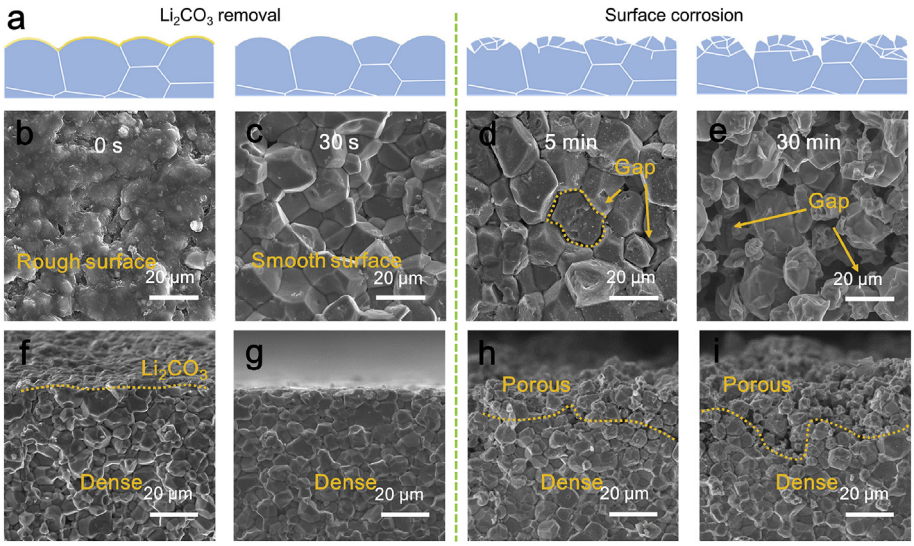

Fig. 2. a) The schematic illustration of interactions between LLZTO and acid. The top-view (b–e) and cross-sectional (f–i) SEM images of LLZTO-air and LLZTO with acid treatment (30 s, 5 min, 30 min).

peaks at ~285.0 and ~290.0 eV in the C 1s spectrum of LLZTO-air pellets corresponded to hydrocarbon contaminations and carbonate species, respectively [26]. The ratio of Li_2CO_3 to the C peak of the LLZTO-air was 54.1%. There was almost no peak at 290.0 eV in the LLZTO-RAT (30 s), showing the complete reaction between Li_2CO_3 and HCl over 30 s. The Li 1s peak at ~55.0 eV and O 1s peak at 531.8 eV were from the surface Li_2CO_3 in the LLZTO-air pellet (Fig. 1f and g). Their positions have been changed to 54.1 and 529.9 eV in the LLZTO-RAT pellet, indicating the photoelectrons were from the Li and O ions in cubic garnet. More obviously, the absent signals of La 3d and Zr 3d in the LLZTO-air spectra intensely appeared in the LLZTO-RAT spectra (Fig. 1h and i). The removal of Li_2CO_3 surface layer successfully disclosed the intrinsic LLZTO.

The morphological changes of LLZTO-air after acid treatment were characterized by scanning electron microscopy (SEM) (Fig. 2a). Fig. 2b shows a rough surface on the LLZTO-air pellet due to Li_2CO_3 contaminant, which is distinct from the typical LLZTO morphology. As the cross-sectional SEM shown in Fig. 2f, the ceramic crystal particles in LLZTO-air were merged together with very low porosity, which is consistent with the measured high relative density of 99.5% [35]. It is worth noting that the fracture section is mostly transgranular, evidencing a relatively high grain boundary adhesion [35]. Under such circumstances, little Li_2CO_3 can be generated inside the pellet, thus achieving a high ionic conductivity. After rapid acid treatment of 30 s, the surface contamination was fully removed. A clear morphology of LLZTO grain particles was disclosed in Fig. 2c, which resembled the fractured cross-section morphology. The whole LLZTO-RAT (30 s) pellet remained dense and compact (Fig. 2g). When the acid treatment length increased to 5 min, some gaps occurred along the grain boundaries on the surface (Fig. 2d). As the cross-sectional SEM image shown in Fig. 2h, roughly the top 5-μm of LLZTO became porous. This could be attributed to the acid corrosion LLZTO after removing Li_2CO_3. The HCl reacted with the LLZTO ceramic by fully H^+/Li^+ exchange, forming soluble chlorides in the HCl solution. And the acid corrosion preferentially occurred at the LLZTO grain boundary compared with the bulk, thus causing gaps along grain boundaries. When increasing the time of acid treatment to 30 min, the surface porosity increased and the depth of corrosion was deepened to 10 μm (Fig. 2e and i).

The ionic conductivities of LLZTO-air pellets before and after acid treatment were compared in Fig. S5. The LLZTO-air showed a high conductivity of 1.6×10^{-3} S cm^{-1} at 30 °C. After rapid acid treatment, the conductivities of LLZTO-RAT (10 s) and LLZTO-RAT (30 s) showed no obvious change, indicating a stable ceramic structure after removing Li_2CO_3 on the surface. The conductivities of LLZTO-RAT (5 min) and LLZTO-RAT (30 min) decreased to 9.1×10^{-4} S cm^{-1} and 6.4×10^{-4} S cm^{-1}, respectively. This could be attributed to the porous LLZTO surface by acid corrosion that weakened the Li^+ migration across boundaries. Considering the completeness of Li_2CO_3 and resulting ionic conductivity, 30 s of acid treatment was determined to be the optimal treating condition. Hereafter, LLZTO-RAT refers to the LLZTO-RAT (30 s) with complete removal of Li_2CO_3, unless otherwise stated.

The intrinsic interface between LLZTO and Li metal was investigated by melting Li metal on the LLZTO pellets at 200 °C. As shown in Figs. S6a and S6b, the wettability of molten Li on LLZTO-air pellet was poor due to the surface Li_2CO_3 layer. After removing the Li_2CO_3, the LLZTO-RAT surface became lithiophilic that was easily wet by molten Li (Fig. S6c). The resulting interface between LLZTO-RAT and Li was tight and free of gaps (Fig. S6d). The interfacial resistance was measured by Electrochemical Impedance Spectroscopy (EIS) in Li/LLZTO-air/Li and Li/LLZTO-RAT/Li symmetric configuration. As shown in Fig. 3a, the initial point of the spectra corresponded to the resistance of the bulk LLZTO electrolyte, and the following semicircle corresponded to the interfacial resistance. Considering charge transfer across two Li/LLZTO interfaces in one symmetric cell, the interfacial resistance determined from the semicircle was divided by two to obtain the value for each Li/LLZTO interface. The interfacial resistance of the Li/LLZTO-RAT was 26 Ω cm^2 at 30 °C, which was 36 times smaller than that of Li/LLZTO-air interface (940 Ω cm^2 at 30 °C in Fig. 3b). The recovery of the intrinsically lithiophilic LLZTO surface by rapid acid treatment rendered a good interface with Li. This intrinsic interface exhibited comparable interfacial resistance to other surface coating (e.g. Al_2O_3, ZnO, Sn) methods (Fig. S7 and Table S1).

Galvanostatic cycling experiments demonstrated the stable and smooth Li^+ transport in the LLZTO-RAT cell. As a control, the Li/LLZTO-air/Li cell showed large overpotential and soon reached short circuit in 5 cycles under 0.1 mA cm^{-2} at 30 °C (Fig. 3c). The poor wetting of Li on the Li_2CO_3 covered LLZTO-air had led to uneven Li plating and stripping. As shown in the cross-sectional SEM image in Fig. 3e, Li dendrite grew along the grain boundary to cause short circuit in the working cell. In comparison, the Li/LLZTO-RAT/Li cells maintained stable cycling over 700 h with a smooth plateau of 19.6 mV under 0.1 mA cm^{-2} at 30 °C (Fig. S8). Similarly, stable cycling performance was shown at 0.2 mA cm^{-2} over 700 h (Fig. 3e), indicating a good Li/LLZTO-RAT interface after eliminating Li_2CO_3 contaminant. And the intrinsic interface with Li metal remained stable during

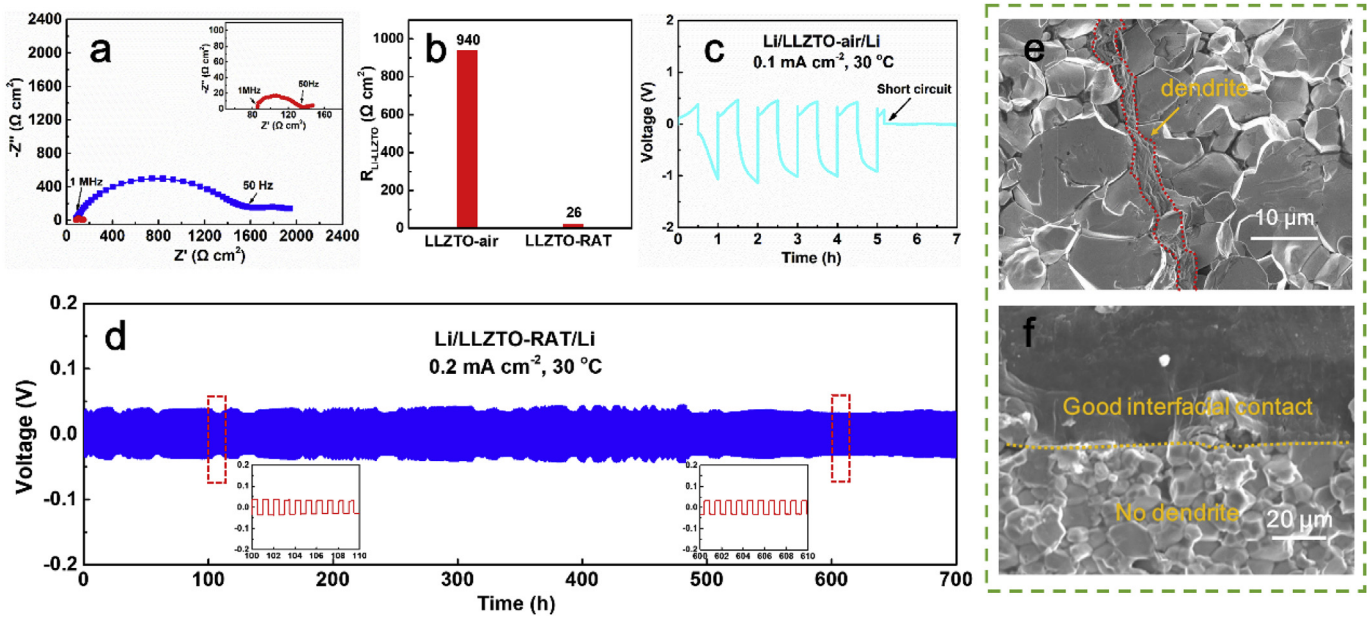

Fig. 3. Comparison of the EIS profiles of Li symmetric cells with LLZTO-air and LLZTO-RAT at 30 °C (inset shows the enlarged impedance curve of the cell with LLZTO-RAT. (b) The interfacial resistances of the Li/LLZTO/Li symmetric cells with LLZTO-air and LLZTO-RAT. c) Galvanostatic cycling performance of Li/LLZTI-air/Li under 0.1 mA cm^{-2} at 30 °C. d) Galvanostatic cycling performance of the Li/LLZTO-RAT/Li under 0.2 mA cm^{-2} at 30 °C. (e) Cross-sectional SEM image of Li/LLZTI-air/Li after short circuit. f) Cross-sectional SEM image of Li/LLZTI-RAT/Li after 700 h cycling.

repeated plating/stripping process (Fig. 3f).

Full SSBs with a Li metal anode and a $LiFePO_4$ (LFP) cathode were constructed using LLZTO-RAT in comparison with LLZTO-air. Fig. 4a shows the schematic configuration of the SSBs. The composite cathode was prepared using ionic liquid as the wetting agent and super P as the conductive additive for room-temperature feasibility [36]. As consistent with the reduced Li/LLZTO-RAT interfacial resistance, the total impedance of the Li/LLZTO-RAT/LFP cell (1978.2 Ω cm^2 at 30 °C) was smaller than that of the Li/LLZTO-air/LFP cell (3513.4 Ω cm^2) (Fig. S9). Correspondingly, the LLZTO-RAT cell showed flat voltage plateaus with smaller polarization than the LLZTO-air cell at different current rates (Fig. 4b). The LLZTO-RAT cell delivered an initial specific discharge capacity of 142.7 mAh g^{-1} with a Coulombic efficiency of 93.3% at 0.1C. The discharge capacities were 132.7, 113.0 and 85.8 mAh g^{-1} at 0.2, 0.5 and 1C, respectively (Fig. 4c). After high-rate cycling, the cell recovered a discharge capacity of 139.4 mAh g^{-1} at 0.1C. The high

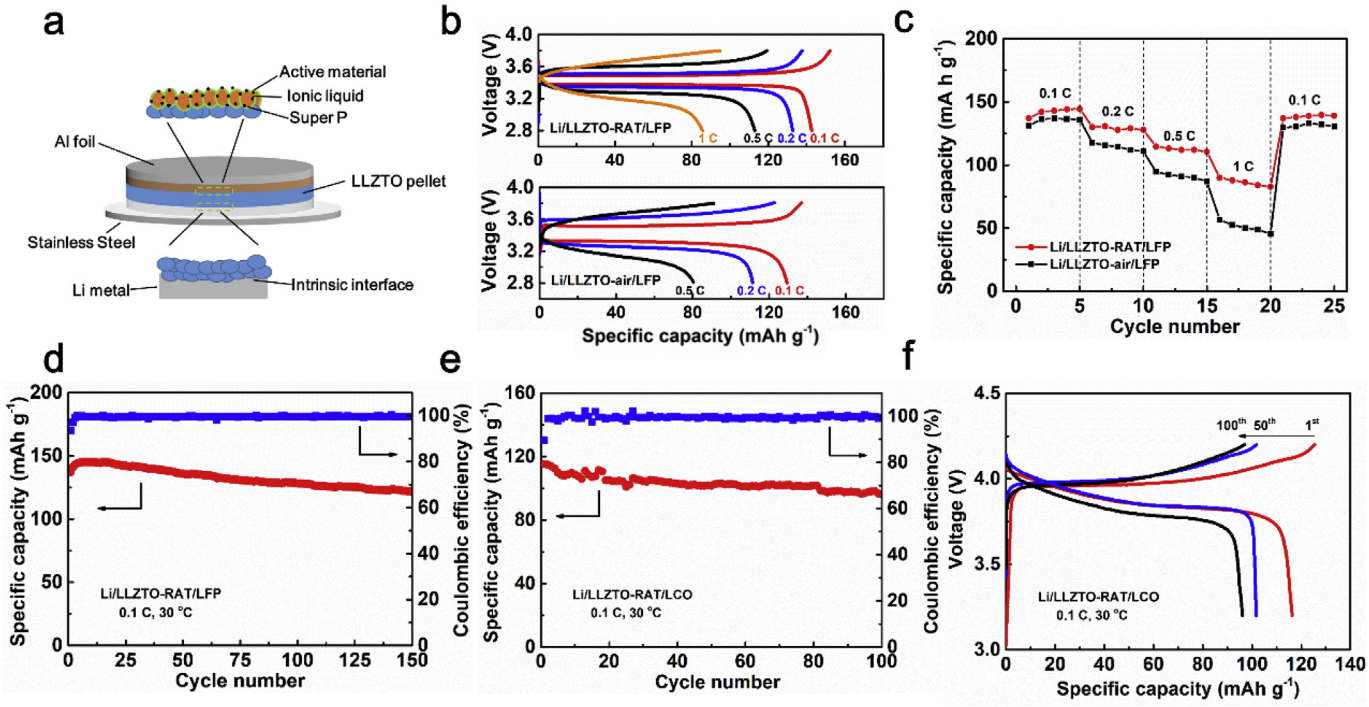

Fig. 4. a) Schematic of SSBs with Li metal anode, LLZTO-RAT electrolyte, and LFP/LCO cathode. b) Charge/discharge curves of Li/LLZTO-RAT/LFP and Li/LLZTO-air/LFP cells at various rate. c) Rate performance of Li/LLZTO-RAT/LFP and Li/LLZTO-air/LFP cells. d) Cycle performance of Li/LLZTO-RAT/LFP under 0.1 C at 30 °C. e) Cycle performance and f) charge/discharge curves of Li/LLZTO-RAT/LCO under 0.1 C at 30 °C.

capacity and excellent rate performance could be attributed to the good interface contact and low interfacial resistance after removing Li_2CO_3 contaminant on the LLZTO-RAT. In contrast, the LLZTO-air cell with less favorable interfaces delivered a discharge capacity of 135.7 mAh g^{-1} with a high overpotential of 0.18 V at 0.1C (Fig. 4b). The discharge capacity decreased to 116.6, 80.9 and 51.4 mAh g^{-1} at 0.2, 0.5 and 1C, respectively. Moreover, the SSB with LLZTO-RAT maintained a capacity retention of 82.1% after 150 cycles at 0.1C and 30 °C (Fig. 4d). To further increase the energy density and power density, SSBs with LLZTO-RAT were also constructed using the $LiCoO_2$ (LCO) cathode. After 100 cycles at 0.1C, the LCO cell remained a discharge capacity of 101.2 mAh g^{-1} and Coulombic efficiency over 99% (Fig. 4f). The charge – discharge curves for 1st, 50^{th} and 100^{th} were shown in Fig. 4e, indicating a stable cycling performance.

The results above demonstrate that the intrinsic Li/LLZTO interface after removing the surface Li_2CO_3 can not only suppress Li dendrite but also enhance the cycling performance of solid-state full cells. This facile method of rapid acid treatment to eliminate Li_2CO_3 can be easily scalable to other acids, such as H_2SO_4 and H_3PO_4. As shown in Fig. S10, after treated with H_2SO_4 and H_3PO_4, the interfacial resistance with Li decreased to 28 Ω cm^2 and 31 Ω cm^2 at 30 °C, respectively. Acid treatment is proved to be an effective way to retrieve the intrinsically lithiophilic LLZTO surface for good compatibility with Li metal. Li symmetric cells exhibited stable cycling over 600 h with no obvious overpotential using LLZTO-RAT by H_2SO_4 and H_3PO_4.

4. Conclusion

In summary, a universal and effective strategy of rapid acid treatment was proposed to remove Li_2CO_3 on the surface of LLZTO, thus retrieving an intrinsic Li/LLZTO interface. Even if the LLZTO pellets were aged in air for 1 month, merely 30 s of HCl (1 M) treatment was enough to clean the surface Li_2CO_3 without damaging the bulk LLZTO. Otherwise, excess treatment with acid could, in turn, corrode the LLZTO pellet and lower the ionic conductivity. Transforming from lithiophobic to lithiophilic, the interfacial resistance of Li/LLZTO was dramatically decreased from 940 to 26 Ω cm^2 at 30 °C. The Li symmetric cells using treated LLZTO can operate over 700 h under 0.2 mA cm^{-2} at 30 °C. Full SSBs with LFP or LCO cathodes delivered excellent rate and cycling performance. These results indicate that such a simple rapid acid treatment successfully discloses the intrinsic lithiophilic LLZTO interface, which can well address the interfacial issue in SSBs by avoiding traditional complex surface coating (e.g. Al_2O_3, ZnO, Sn). The acid treatment also can be easily scalable to various strong or weak acid, such as H_2SO_4 and H_3PO_4, which are supposed to obtain the same excellent electrochemical performance with HCl treatment.

Acknowledgements

The authors would like to thank the National Natural Science Foundation of China (Grant No. 51771222, 51532002, 51772314 and 51702346), the National Key R&D Program of China (Grant No. 2018YFB0104300), the “Taishan Scholars Program”, Natural Sciences and Engineering Research Council of Canada (NSERC), Canada Research Chair Program (CRC), and University of Western Ontario.

Appendix A. Supplementary data

Supplementary data to this article can be found online at https://doi.org/10.1016/j.nanoen.2019.04.058.

References

[1] J.M. Tarascon, M. Armand, Nat 414 (2001) 359–367.
[2] A. Manthiram, X. Yu, S. Wang, Nat. Rev. Mater. 2 (2017).
[3] F. Zheng, M. Kotobuki, S.F. Song, M.O. Lai, L. Lu, J. Power Sources 389 (2018) 198–213.
[4] N.J. Dudney, J.B. Bates, R.A. Zuhr, C.F. Luck, J.D. Robertson, Solid State Ionics 53 (1992) 655–661.
[5] Y. Inaguma, L.Q. Chen, M. Itoh, T. Nakamura, T. Uchida, H. Ikuta, M. Wakihara, Solid State Commun. 86 (1993) 689–693.
[6] J.B. Goodenough, H.Y.P. Hong, J.A. Kafalas, Mater. Res. Bull. 11 (1976) 203–220.
[7] Y. Liu, Q. Sun, Y. Zhao, B. Wang, P. Kaghazchi, K.R. Adair, R. Li, C. Zhang, J. Liu, L.-Y. Kuo, ACS Appl. Mater. Interfaces 10 (2018) 31240–31248.
[8] J.H. Kennedy, S. Sahami, S.W. Shea, Z.M. Zhang, Solid State Ionics 18–19 (1986) 368–371.
[9] R. Murugan, V. Thangadurai, W. Weppner, Angew. Chem. Int. Ed. 46 (2007) 7778–7781.
[10] B.M. Al-Abdullah, M.M. Angor, K.M. Al-Ismail, R.Y. Ajo, Ital. J. Food Sci. 23 (2011) 331–337.
[11] V. Thangadurai, D. Pinzaru, S. Narayanan, A.K. Baral, J. Phys. Chem. Lett. 6 (2015) 292–299.
[12] M. Kotobuki, H. Munakata, K. Kanamura, Y. Sato, T. Yoshida, J. Electrochem. Soc. 157 (2010) A1076–A1079.
[13] C.W. Ahn, J.J. Choi, J. Ryu, B.D. Hahn, J.W. Kim, W.H. Yoon, J.H. Choi, J.S. Lee, D.S. Park, J. Power Sources 272 (2014) 554–558.
[14] J. Liang, Q. Sun, Y. Zhao, Y. Sun, C. Wang, W. Li, M. Li, D. Wang, X. Li, Y. Liu, J. of Mater. Chem. A. 6 (2018) 23712–23719.
[15] R.H. Basappa, T. Ito, H. Yamada, J. Electrochem. Soc. 164 (2017) A666–A671.
[16] E.J. Cheng, A. Sharafi, J. Sakamoto, Electrochim. Acta 223 (2017) 85–91.
[17] T. Kato, R. Yoshida, K. Yamamoto, T. Hirayama, M. Motoyama, W.C. West, Y. Iriyama, J. Power Sources 325 (2016) 584–590.
[18] W. Luo, Y. Gong, Y. Zhu, K.K. Fu, J. Dai, S.D. Lacey, C. Wang, B. Liu, X. Han, Y. Mo, E.D. Wachsman, L. Hu, J. Am. Chem. Soc. 138 (2016) 12258–12262.
[19] K.K. Fu, Y. Gong, Z. Fu, H. Xie, Y. Yao, B. Liu, M. Carter, E. Wachsman, L. Hu, Angew. Chem. Int. Ed. Engl. 56 (2017) 14942–14947.
[20] M.H. He, Z.H. Cui, C. Chen, Y.Q. Li, X.X. Guo, J. Mater. Chem. 6 (2018) 11463–11470.
[21] C. Wang, Y. Gong, B. Liu, K. Fu, Y. Yao, E. Hitz, Y. Li, J. Dai, S. Xu, W. Luo, E.D. Wachsman, L. Hu, Nano Lett. 17 (2017) 565–571.
[22] X. Han, Y. Gong, K.K. Fu, X. He, G.T. Hitz, J. Dai, A. Pearse, B. Liu, H. Wang, G. Rubloff, Y. Mo, V. Thangadurai, E.D. Wachsman, L. Hu, Nat. Mater. 16 (2017) 572–579.
[23] L. Cheng, E.J. Crumlin, W. Chen, R. Qiao, H. Hou, S. Franz Lux, V. Zorba, R. Russo, R. Kostecki, Z. Liu, K. Persson, W. Yang, J. Cabana, T. Richardson, G. Chen, M. Doeff, Phys. Chem. Chem. Phys. 16 (2014) 18294–18300.
[24] A. Sharafi, S.H. Yu, M. Naguib, M. Lee, C. Ma, H.M. Meyer, J. Nanda, M.F. Chi, D.J. Siegel, J. Sakamoto, J. Mater. Chem. 5 (2017) 13475–13487.
[25] A. Sharafi, E. Kazyak, A.L. Davis, S. Yu, T. Thompson, D.J. Siegel, N.P. Dasgupta, J. Sakamoto, Chem. Mater. 29 (2017) 7961–7968.
[26] Y. Li, X. Chen, A. Dolocan, Z. Cui, S. Xin, L. Xue, H. Xu, K. Park, J.B. Goodenough, J. Am. Chem. Soc. 140 (2018) 6448–6455.
[27] I. Garbayo, M. Struzik, W.J. Bowman, R. Pfenninger, E. Stilp, J.L. Rupp, Adv. Energy Mater. 8 (2018) 1702265.
[28] F.M. Du, N. Zhao, Y.Q. Li, C. Chen, Z.W. Liu, X.X. Guo, J.l of Power Sources 300 (2015) 24–28.
[29] Y. Li, Z. Wang, Y. Cao, F. Du, C. Chen, Z. Cui, X. Guo, Electrochim. Acta 180 (2015) 37–42.
[30] C. Ma, E. Rangasamy, C. Liang, J. Sakamoto, K.L. More, M. Chi, Angew. Chem. Int. Ed. 54 (2015) 129–133.
[31] A. Sharafi, S. Yu, M. Naguib, M. Lee, C. Ma, H.M. Meyer, J. Nanda, M. Chi, D.J. Siegel, J. Sakamoto, J. Mater. Chem. 5 (2017) 13475–13487.
[32] W. Xia, B. Xu, H. Duan, X. Tang, Y. Guo, H. Kang, H. Li, H. Liu, J. Am. Ceram. Soc. 100 (2017) 2832–2839.
[33] Y. Li, B. Xu, H. Xu, H. Duan, X. Lu, S. Xin, W. Zhou, L. Xue, G. Fu, A. Manthiram, J.B. Goodenough, Angew. Chem. Int. Ed. Engl. 56 (2017) 753–756.
[34] C. Liu, K. Rui, C. Shen, M.E. Badding, G. Zhang, Z. Wen, J. Power Sources 282 (2015) 286–293.
[35] M. He, Z. Cui, C. Chen, Y. Li, X. Guo, J. Mater. Chem. 6 (2018) 11463–11470.
[36] Y. Shao, H. Wang, Z. Gong, D. Wang, B. Zheng, J. Zhu, Y. Lu, Y.-S. Hu, X. Guo, H. Li, ACS Energy Lett 3 (2018) 1212–1218.

Hanyu Huo is currently a Ph.D. candidate at State Key Laboratory of High Performance Ceramics and Superfine Microstructure, Shanghai Institute of Ceramics, Chinese Academy of Sciences (SICCAS), China. At the same time, he is a visiting student in Prof. Xueliang (Andy) Sun's Nanomaterials and Energy Group at University of Western Ontario, Canada. He got his B.S. degree in Inorganic Materials Technology from School of Materials Science and Technology, Shandong University, in 2015. Currently, his research interests focus on solid-state batteries and Li metal batteries.

Yue Chen is a master student at State Key Laboratory of High Performance Ceramics and Superfine Microstructure, Shanghai Institute of Ceramics, Chinese Academy of Sciences (SICCAS), China. He received his B.S. degree from China Jiliang University in 2016. Now, his research interests mainly focus on solid-state electrolytes and rechargeable all-solid-state batteries.

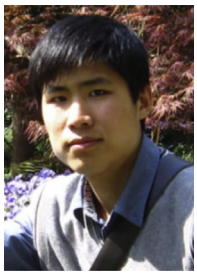

Ning Zhao received his Ph.D. in material physics and chemistry from Shanghai Institute of Ceramics, Chinese Academy of Sciences (SICCAS), under the supervision of Prof. Xiangxin Guo. Ning Zhao has been actively involved in Li-O_2 battery researches, and the fundamental researches on Na-O_2 battery. His current research focuses on solid-state electrolytes and rechargeable all-solid-state batteries.

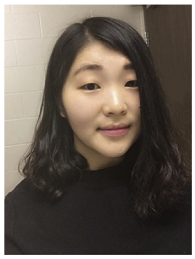

Xiaoting Lin is currently a Ph.D. candidate in Prof. Xueliang (Andy) Sun's group at the University of Western Ontario, Canada. She received her B.S. degree in Applied chemistry in 2012 from Liaocheng University and obtained her M.S. degree in Physical Chemistry in 2016 from Ningbo University. Currently, her research interests focus on development of advanced nanomaterials for Na-O_2 batteries as well as solid-state Na-O_2 batteries.

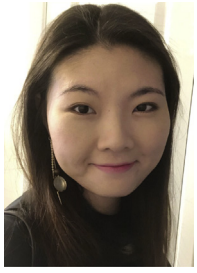

Jing Luo received her B.S. degree in Chemical Engineering from the University of Illinois—Urbana Champaign (U.S.A.) in 2013 and M.S. degree under the supervision of Prof. Nae-Lih Wu from National Taiwan University (Taiwan) in 2016. She is now pursuing her Ph.D. degree in Prof. Xueliang (Andy) Sun's group at University of Western Ontario, Canada. Her current research interests focus on atomic layer deposition in the application of Li-ion batteries and polymer based solid-state batteries.

Xiaofei Yang is currently a postdoctoral associate in Prof. Xueliang (Andy) Sun's Nanomaterials and Energy Group. He received his B.E. degree in Chemical Engineering from Anhui University, China, in 2013 and Ph.D degree in Dalian Institute of Chemcial Physics, Chinese Academy of Sciences, China, in 2018 under the supervision of Prof. Huamin Zhang. His research interests focus on Li-S batteries, all-solid-state Li-ion and Li-S batteries, and battery interface studies via synchrotron X-ray characterizations.

Yulong Liu is currently associate professor at Northeast Normal University, China. Before working in Northeast Normal University, he was a postdoctoral fellow in Prof. Xueliang (Andy) Sun's Nanomaterials and Energy Group. He received his Bachelor degree from Central South University, China, in 2010, and Master degree in 2013. In 2017, he obtained his Ph.D. degree in Materials Science and Engineering from University of Western Ontario. His research interests include nanomaterials for lithium ion batteries, especially $LiFePO_4$ (in collaboration with *Johnson Matthey Inc*., previous Phostech), and the development of the high energy density solid-state batteries with GLABAT Solid State Battery Inc.

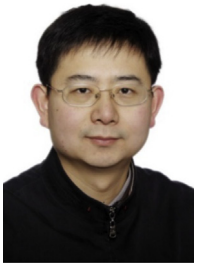

Xiangxin Guo received his Ph.D. from Institute of Physics, Chinese Academy of Sciences (CAS) in 2000. As a postdoctoral scientist, he continued research at the Max Planck Institute for Solid State Research, at the Paul Drude Institute for Solid State Electronics, and at the European Synchrotron Radiation Facility. He then worked as a staff scientist at the Max Planck Institute, before joining the Shanghai Institute of Ceramics. He is currently a full professor at College of Physics, Qingdao University under the funding of "Taishan Scholars Program". His research focuses on solid garnet batteries, metal-air batteries, and heterostructure-based solid-state ionic devices.

Xueliang (Andy) Sun is a Canada Research Chair in Development of Nanomaterials for Clean Energy, Fellow of the Royal Society of Canada and Canadian Academy of Engineering and Full Professor at the University of Western Ontario, Canada. Dr. Sun received his Ph.D. in materials chemistry in 1999 from the University of Manchester, UK, which he followed up by working as a postdoctoral fellow at the University of British Columbia, Canada and as a Research Associate at L'Institut National de la Recherche Scientifique (INRS), Canada. His current research interests are focused on advanced materials for electrochemical energy storage and conversion.